AGU ADVANCING EARTH AND SPACE SCIENCES

Geophysical Research Letters

RESEARCH LETTER
10.1029/2025GL116590

Special Collection:
Science from the Surface Water and Ocean Topography Satellite Mission

Evaluating SWOT in the Coastal Zone: Comparisons With Tide Gauge and Airborne LiDAR in the Bristol Channel and Severn Estuary, UK

Youtong Rong[1], Paul Bates[1,2], Jeff Neal[1], Paul Bell[3], Christine Gommenginger[4], Ian Dougal Lichtman[3], Christopher Banks[3], Francisco J. M. Calafat[3], Adrien Martin[4,5], Jennifer Brown[4], Richard Cooke[3], Christopher Balfour[3], Michela De Dominicis[3], Marta Payo Payo[3], Simon Williams[3], Laurent Amoudry[3], Stephen Chuter[2], Simon Neill[6], Jude Chisholm[6], Colin J. Gleason[7], John Kupiec[8], and Matt Lewis[9]

[1]School of Geographical Sciences, University of Bristol, Bristol, UK, [2]Fathom, Bristol, UK, [3]National Oceanography Centre, Liverpool, UK, [4]National Oceanography Centre, Southampton, UK, [5]NOVELTIS, Labège, France, [6]School of Ocean Sciences, Bangor University, Menai Bridge, UK, [7]Department of Civil and Environmental Engineering, University of Massachusetts, Amherst, MA, USA, [8]Geomatics Unit, The Environment Agency, Rivers House, Bath, UK, [9]Clean Energy Team, Wood plc, Glasgow, UK

Abstract Traditional nadir altimeters struggle with coastal water surface elevation (WSE) measurement and fine-scale river-estuary interactions, due to land-water signal interference and their wide inter-track spacing. The wide-swath Surface Water and Ocean Topography (SWOT) mission, using a new Ka-band radar interferometer, aims to address these issues by delivering 2D WSE measurements with unprecedented spatial resolution, accuracy, and precision. However, the mission's effectiveness in coastal WSE retrieval and its error characteristics remain unverified. This study leverages gauge and airborne LiDAR data to validate SWOT's WSE in the Bristol Channel and Severn Estuary. Assuming error-free in situ data, SWOT ocean products exhibit a standard deviation of difference (STD) of 13 cm within a 3 km radius of tide gauges. Compared to LiDAR, SWOT's PIXC measurements have STD of 37 cm, improving to 14 cm over 100 m grids and 9 cm over 1 km^2 areas. This meets the SWOT science requirement of 10 cm STD at 1 km^2 scale and extends satellite-based WSE monitoring into complex coastal environments.

Plain Language Summary Conventional radar altimeters struggle within 5–10 km of shorelines due to land-water interference, large footprints, and wide inter-track spacing. While SAR-mode altimetry and waveform retracking improve near-shore (1–5 km) coverage, residual errors, and inter-track gaps limit fine-scale coastal applications. Surface Water and Ocean Topography (SWOT)'s Ka-band radar interferometry promises to overcome these limitations, delivering wide-swath water surface elevation (WSE) monitoring in complex coastal systems. We validated SWOT during its March–July 2023 Calibration/Validation (Cal/Val) phase in the macro-tidal Bristol Channel using ADCP-mounted pressure sensors, tide gauges, and ~446 million airborne LiDAR points under varying tidal conditions. Spatial aggregation with quality control produces accurate WSE estimates despite high pixel-level variability, demonstrating SWOT's capability to capture coastal hydrodynamics and extend reliable WSE observations into challenging coastal environments.

Key Points:

- First validation of Surface Water and Ocean Topography (SWOT) in a coastal environment using concurrent LiDAR, tide gauge, and pressure gauge across the Cal/Val phase
- SWOT's spatial and temporal validation reveals high accuracy water level measurements across diverse tidal conditions
- SWOT water surface elevations show directional-dependent errors, which are correlated with the viewing geometry and influenced by local coastal morphology

Supporting Information:

Supporting Information may be found in the online version of this article.

Correspondence to:

P. Bates,
Paul.Bates@bristol.ac.uk

Citation:

Rong, Y., Bates, P., Neal, J., Bell, P., Gommenginger, C., Lichtman, I. D., et al. (2026). Evaluating SWOT in the coastal zone: Comparisons with tide gauge and airborne LiDAR in the Bristol Channel and Severn Estuary, UK. *Geophysical Research Letters*, *53*, e2025GL116590. https://doi.org/10.1029/2025GL116590

Received 8 MAY 2025
Accepted 4 DEC 2025

Author Contributions:

Conceptualization: Paul Bates, Jeff Neal, Paul Bell, Christine Gommenginger, Jennifer Brown, Simon Neill, Matt Lewis
Formal analysis: Youtong Rong, Jeff Neal, Paul Bell, Ian Dougal Lichtman, Christopher Banks, Stephen Chuter, Simon Neill, Jude Chisholm, Colin J. Gleason

1. Introduction

Rising sea levels and increasingly frequent storm surges, exacerbated by climate change, are profoundly impacting human activities and coastal ecosystems (Calafat et al., 2022; Schuerch et al., 2018). While the impacts of the growing frequency and devastation of climate hazards are being disproportionately felt in coastal cities (Hauer et al., 2021; Jafarzadegan et al., 2023), the sparsity of in situ gauge data contrasts sharply with the rising demand for precise and timely coastal sea level information (Toimil et al., 2023). The sparse distribution of tide gauges, often located in sheltered environments unrepresentative of offshore conditions, and restricted data availability hinder their utility in monitoring fine-scale coastal water dynamics (Vignudelli et al., 2019). Satellite altimeter missions, initially designed for open-ocean applications (Fu & Cazenave, 2000), have emerged as a promising alternative for offshore water level measurement (Alsdorf et al., 2007). However, conventional nadir altimeters are suboptimal for capturing near-coastal zone surface water dynamics, given their low temporal (10–35 days) and spatial (70–600 m) resolutions, significant vertical errors ranging from decimeters to meters

Funding acquisition: Paul Bates, Jeff Neal, Paul Bell, Christine Gommenginger, Jennifer Brown, Laurent Amoudry, Simon Neill, John Kupiec, Matt Lewis
Investigation: Paul Bates, Jeff Neal, Ian Dougal Lichtman, Francisco J. M. Calafat, Adrien Martin, Richard Cooke, Christopher Balfour, Michela De Dominicis, Marta Payo Payo, Simon Williams, Stephen Chuter, Simon Neill
Methodology: Youtong Rong, Paul Bates, Jeff Neal, Paul Bell, Ian Dougal Lichtman, Stephen Chuter, Simon Neill, Matt Lewis
Project administration: Jeff Neal, Paul Bell, Simon Neill
Resources: Paul Bell, John Kupiec
Supervision: Paul Bates, Jeff Neal, Paul Bell, Simon Neill
Validation: Youtong Rong, Paul Bates, Paul Bell, Ian Dougal Lichtman
Visualization: Youtong Rong, Ian Dougal Lichtman, Stephen Chuter, Simon Neill, Jude Chisholm, Colin J. Gleason
Writing – original draft: Youtong Rong
Writing – review & editing: Youtong Rong, Paul Bates, Jeff Neal, Paul Bell, Ian Dougal Lichtman, Christopher Banks, Adrien Martin, Jennifer Brown, Stephen Chuter, Simon Neill, Jude Chisholm, Colin J. Gleason, John Kupiec, Matt Lewis

(Altenau et al., 2017; O'Loughlin et al., 2016), and substantial gaps between orbital tracks. The altimeter data are further compromised by waveform variability, surrounding land elevations, and specular reflections, resulting in a dramatic decrease in valid water surface elevation (WSE) measurements when approaching coastal areas (Laignel et al., 2015; Vignudelli et al., 2019). Whilst advances in SAR altimetry (~300 m along-track resolution) and waveform retracking have improved WSE retrieval to within 1–5 km of coastline (Birol et al., 2021; Dinardo et al., 2018; Peng et al., 2024; Schlembach et al., 2022), residual errors and inter-track gaps limit current altimetry for many scientific and practical applications. Enhancing coastal observation capabilities within 10 km of shorelines is increasingly recognized as a priority (Cipollini et al., 2017).

The Surface Water and Ocean Topography (SWOT) mission, launched in December 2022 and featuring an advanced Ka-band Radar Interferometer (KaRIn), marks a significant step forward in extending satellite-based WSE observations into challenging coastal environments. With its 120 km swath width, SWOT enables detailed spatial characterization (~10–60 m resolution) of water dynamics, targeting WSE measurements with <10 cm accuracy when averaged over a 1 km^2 area (Fu et al., 2024). While extensive validation of SAR-mode altimetry has established its accuracy through crossover analysis and tide gauge comparisons (Dinardo et al., 2021; Fenoglio et al., 2021; Kleinherenbrink et al., 2020), validating SWOT's wide-swath interferometry in macro-tidal coastal environments presents new challenges. This requires high-quality reference data sharing the same location and reference frame but with superior vertical accuracy, given the limited in situ observations capable of capturing coastal spatiotemporal variability. Traditionally, validation relies on independent data sets, such as comparisons with other satellite altimetry missions at crossover points or with in situ measurements from nearby sites (Hart-Davis et al., 2024; Turki et al., 2015). However, comparing single-point gauge measurements to high-resolution elevation fields is problematic in coastal areas with substantial WSE variability (Turki et al., 2015). Whilst Salameh et al. (2024) have compared LiDAR and SWOT derived DEMs over inter-tidal areas and Lichtman et al. (2025) provide detailed KaRIn versus tide gauge comparisons, thorough effort comparing SWOT WSE with concurrent airborne LiDAR and gauges has not yet been conducted in the coastal zone. To bridge this gap, this study leverages tide gauge, ADCP-mounted pressure sensor and airborne LiDAR data to validate SWOT's performance in the Bristol Channel.

2. Methodology

2.1. Study Area

The Bristol Channel and Severn Estuary in the UK's southwest forms a large macro-tidal estuary with the world's second-largest tidal range (~14 m). The estuary's funnel-shaped morphology (100 km long, 1–20 km wide) and distinctive bathymetry—featuring gentle slopes and a deeper central channel (Figure 1a and Figure S1 in Supporting Information S1)—amplify tidal energy, generating powerful currents, high turbidity, and regular tidal bores (Hart-Davis et al., 2024). Wind- and pressure-driven surges, along with river discharge, further modulate these dynamics (Uncles, 2010); their interaction, exacerbated by sea-level rise, determines extreme water levels and flood risk, necessitating continuous, high-resolution monitoring (Lyddon et al., 2018). Covered by SWOT's 90-day daily fast-sampling orbit (Cal/Val phase, March–July 2023), overlapping swaths here deliver the equivalent of ~3 years of the following standard science-mode passes (1–7+ per 21-day cycle). While standard LiDAR pulses are typically absorbed by water due to its transparency, lack of visual key points, and smooth surface, the sediment-rich waters of the Bristol Channel reflect near-nadir LiDAR pulses back to the sensor. Depending on factors such as sensor type, flight altitude, and incidence angle, the reflected intensity values over the site generally range from 100 to 1,000 (compared to 1,000–4,000 over land), facilitating relatively dense WSE measurements. Figure 1a shows the SWOT swath coverage over the Bristol Channel acquired during pass 42 (blue squares), highlighting tiles 063R and 064R (red squares). A 500 m resolution NEMO-UK500 hydrodynamic model (covering the UK coastal strip, under development in the CHAMFER project, see Supporting Information S1) was used to temporally correct the LiDAR data to the SWOT overpass time. Figure 1b shows LiDAR-derived WSE, and Figures 1c–1e present SWOT data sets used for validation: the SWOT High Rate Water Mask Pixel Cloud (PIXC Version C, SWOT, 2024a), the 100 m Raster (Raster Version C, SWOT, 2024b), and the 250 m L3 Low Rate Unsmoothed Sea Surface Height (SSH Version 2.0.1, AVISO/DUACS, 2025), respectively. The SSH data measures ocean surface height equivalent to inland high-rate WSE but uses low-rate data streaming and a different processing approach.

10.1029/2025GL116590

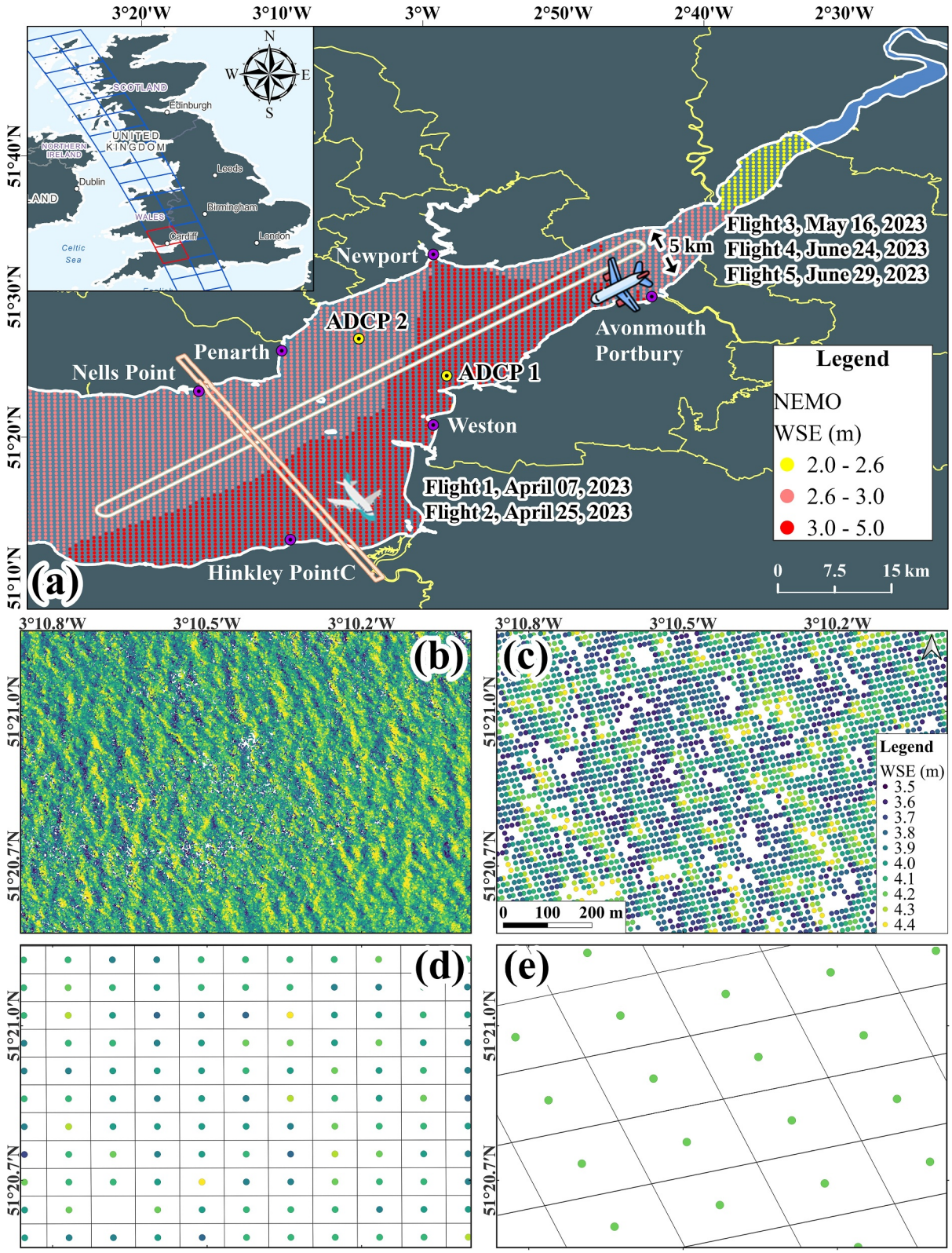

Figure 1. Bristol Channel and Severn Estuary study area. (a) Location map showing NEMO-UK500 tidal elevation on 24 June 2023, with tide gauge (purple), ADCP (yellow), and LiDAR survey extent (white/orange rectangles). (b–e) Show water surface elevation captured by LiDAR, Surface Water and Ocean Topography PIXC, Raster, and Unsmoothed Sea Surface Height, respectively.

2.2. SWOT Data

Validation used three SWOT data sets: PIXC, Raster, and Unsmoothed SSH. The PIXC product provides adaptively averaged, ellipsoid-relative WSE at ∼10–60 m resolution, using the *geolocation_qual* bitwise flag for data quality. The Raster product aggregates pixel measurements onto a uniform 100 m grid to mitigate random noise, with the *wse_qual* aggregated flag as quality indicator. Bitwise flags contain granular information (up to 31 bits) enabling superior quality control compared to aggregated flags, though initial assessment with aggregated flags is recommended before detailed bitwise analysis.

The L3 Unsmoothed SSH data set is derived from the corresponding L2 product by integrating KaRIn measurements and nadir altimetry data, reducing noise and filling data gaps through a multi-mission framework that incorporates data from ∼20 satellite missions (Dibarboure et al., 2024). To ensure compatibility with the in situ gauge data, which measures tide and atmospheric pressure effects, the Total Water Level was calculated from the sea surface height anomaly (Equation 1). This calculation utilized the corrections provided with the SWOT Unsmoothed data, resulting in a data set that matches the tide gauges.

$$\text{Total Water Level} = \text{Sea Surface Height Anomaly} + \text{Ocean tide} + \text{Mean Sea Surface} + \text{Dynamic Atmospheric Correction} \quad (1)$$

2.3. Tide Gauge and ADCP-Mounted Pressure Sensors

Figure 1a illustrates the water level monitoring network along the Bristol Channel coastlines, comprising four gauges that have recorded high-frequency measurements at 10–15 min intervals (Environment Agency, 2024; Lichtman et al., 2024). To address spatial coverage gaps, two additional GNSS-Interferometric Reflectometry gauges (Williams et al., 2020) were installed at Nells Point and Weston-super-Mare (Weston). Overall, the gauge network's leveling accuracy is better than 0.1 m, while GNSS-equipped gauges deliver even higher precision (https://www.ordnancesurvey.co.uk/geodesy-positioning/os-net/accuracy). Two seabed-mounted ADCPs (Sentinel V20) equipped with pressure sensors were deployed offshore to capture instantaneous SSH measurements, each providing a 0–300 m measurement range with 0.1% full-scale accuracy.

2.4. Airborne LiDAR Surveys

Five airborne LiDAR surveys were conducted between April and June 2023, using two airborne LiDAR systems collecting high-accuracy WSE measurements (∼0.5 m resolution) coincident with SWOT overpasses. These measurements encompassed a wide range of tidal conditions, from low tides at −5.1 m relative to the EGM2008 geoid to high tides reaching +5.4 m and including both incoming and outgoing tides (Table S1 in Supporting Information S1). As shown in Figure 1a, three along-estuary flights on 16 May, 24 June, and 29 June were orientated longitudinal to the estuary along a 55 km track and utilized a Leica Hyperon LiDAR system. The remaining two cross-estuary flights on 7 and 25 April were orientated perpendicular to the estuary along a 35 km track, utilizing a Leica T500 LiDAR system. Each flight lasted up to 20 min with a ∼1 km swath width at ∼3 km altitude, achieving point densities of 4–10 points/m^2. Validation against 549 UK Environment Agency ground-control points showed Root Mean Squared Error (RMSE) below 15 cm and STD under 10 cm across terrestrial targets. Theoretically, individual LiDAR returns are expected to have error budgets within 10 cm (Zlinszky et al., 2017) and this has previously been found to be the case in multiple validation studies with the above two instruments.

2.5. LiDAR and Gauge Data Processing

For accurate spatial alignment with SWOT data, gauge and LiDAR measurements were transformed from Ordnance Datum Newlyn (ODN) orthometric heights to EGM2008 geoid heights using PyProj (v3.6.1) and Ordnance Survey National Transformation version 2 grids. While the tool's accuracy is not validated beyond 1–2 km offshore (Greaves, 2016), it remains the best available method for converting ODN orthometric heights to geodetic heights. Additionally, abnormal LiDAR points, such as those representing island surfaces and boat reflections significantly higher than their surroundings, were filtered out using a coastline mask and some manual processing. Data with elevations >6 m or <−6 m were rejected as outside expected water levels for the survey

periods. This approach confined the validation to open water surfaces, thereby avoiding comparisons over land (including small islands and areas within 50 m of the shore).

All tide gauge data sampled at 10–15 min intervals were temporally interpolated to match the timing of SWOT overpasses using MATLAB's modified Akima method, which effectively handles both curved and flat segments typical of riverine or intertidal sites (Lichtman et al., 2025). For seabed-mounted ADCP moorings, 2 Hz pressure measurements from Sentinel V20 ADCP sensors were processed to derive 10-min mean SSH. Atmospheric pressure was corrected using data from nearby Penarth and Weston stations, assuming constant seawater density due to limited ancillary profiles. The 10-min mean immediately preceding each SWOT overpass was used for validation, as high-frequency fluctuations preclude reliable interpolation, unlike tide gauge measurements. In contrast, synchronizing LiDAR measurement with the SWOT overpass is challenging. LiDAR surveys (~20 min) only partially overlap with the SWOT's 21-s data collection period, and high tidal variability during this window (up to 60 cm) complicates direct comparisons. To address this, NEMO-UK500 hydrodynamic model tidal elevations were used for temporal alignment, providing predictions every 10 min at 500 m intervals across the estuary. Over the five-flight survey, NEMO-UK500 compared to SWOT Raster data shows a STD of 0.15 m and a bias of −0.35 m, systematically underestimating water levels relative to both SWOT and tide gauges (Figure S2 in Supporting Information S1). These discrepancies partly reflect that SWOT records total water levels while NEMO-UK500 used in the paper represents tidal elevation only (excluding surge and river influences). However, since only relative SSH changes are required to adjust the LiDAR-derived WSE, a linear regression was applied to interpolate and extrapolate the NEMO-UK500 data, aligning the LiDAR WSE with the SWOT overpass time.

To address spatial resolution differences, LiDAR points within each 100 m raster cell were averaged for grid-by-grid comparison. For PIXC, given variable pixel footprints, LiDAR data were aggregated using four radius buffers (10–40 m) centered on each pixel. For comparing SWOT SSH with tide gauges, all SSH data within a 3-km radius of each gauge were compiled, and the median total water level for each overpass was compared against the corresponding gauge observation (Lichtman et al., 2025). The within-radius standard deviation, relative to each median, remained below 0.1 m for most overpasses. The 3-km radius was selected to account for potential spatial variability in the SWOT observations while maintaining proximity to the gauge location, given the observed phase lag discrepancies between SWOT and gauge measurements (Hart-Davis et al., 2024). Median values were used to reduce outlier influence, particularly near land-sea interfaces where degraded altimeter data quality can occur. For offshore SSH comparison, ADCP-derived water levels were directly compared with corresponding SSH grids.

The error metrics included are the RMSE, STD, Bias, and the coefficient of determination (R^2). For data sets $X = \{x_1, x_2, \ldots, x_n\}$ and $Y = \{y_1, y_2, \ldots, y_n\}$,

$$\begin{aligned} \mathbf{RMSE} &= \sqrt{\frac{1}{n}\sum_{i=1}^{n}(x_i - y_i)^2} \\ \mathbf{STD} &= \sqrt{\frac{1}{n-1}\sum_{i=1}^{n}(d_i - \overline{d})^2} \\ \mathbf{Bias} &= \frac{1}{n}\sum_{i=1}^{n} d_i \\ \boldsymbol{R^2} &= 1 - \frac{\sum_{i=1}^{n}(x_i - y_i)^2}{\sum_{i=1}^{n}(y_i - \overline{y})^2} \end{aligned} \tag{2}$$

where $d_i = x_i - y_i$ and $\overline{d}$ is the mean of d_i (Bias).

3. Results

3.1. Temporal Comparison Between Gauge and SWOT Total Water Level

SWOT's temporal capabilities for monitoring coastal water dynamics were validated using six tide gauges (98 measurements) and two pressure gauges (58 measurements) from March to July 2023. Data limitations arose from fill values in the original SWOT SSH data set, with missing reference surface data in high-latitude and

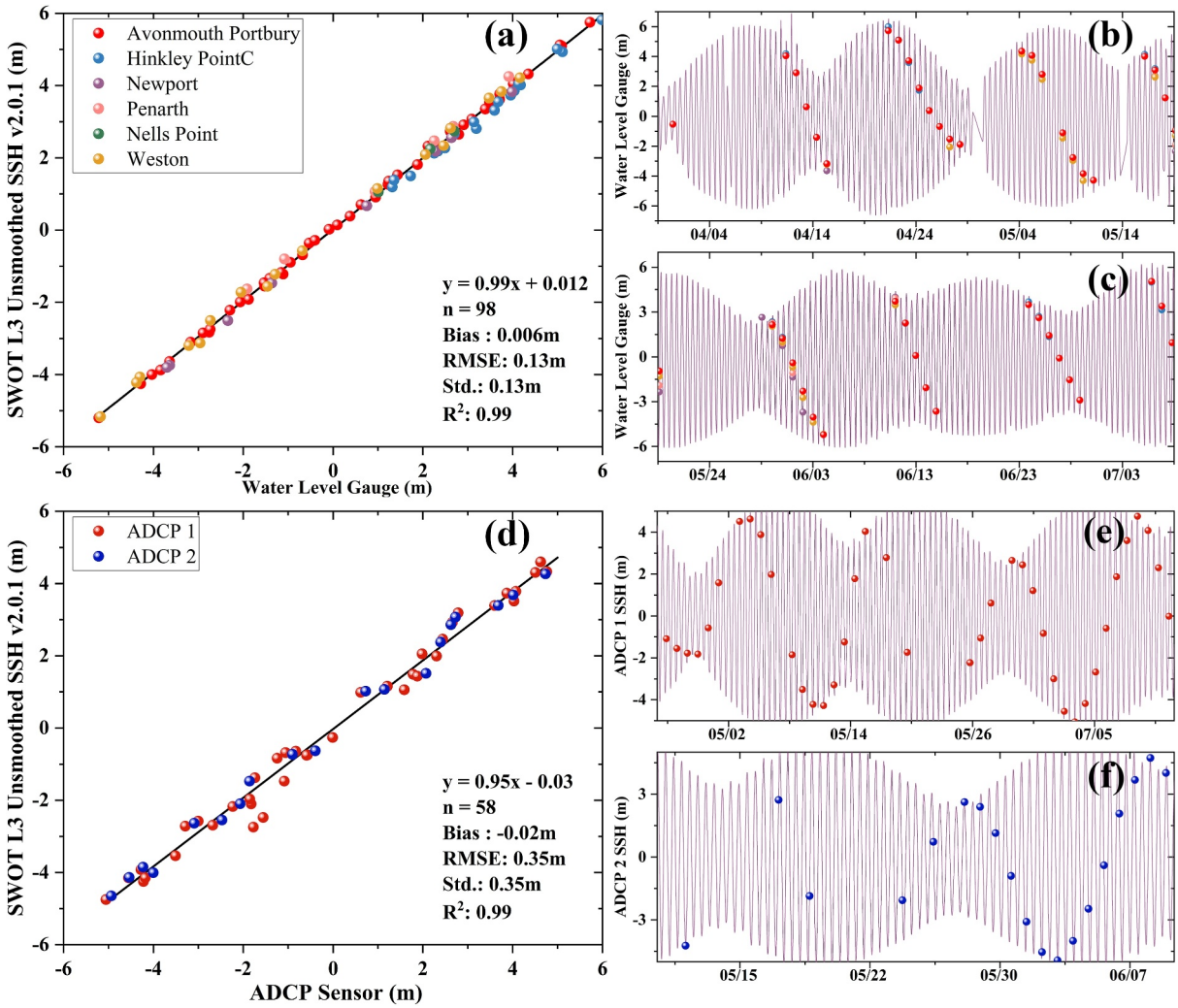

Figure 2. Surface Water and Ocean Topography coastal water dynamics monitoring evaluation. (a) SWOT-derived water surface elevation (WSE) compared with tide gauge data. (d) SWOT-derived WSE compared with ADCP-mounted pressure sensor data. Panels (b, c) and (e, f) show time periods for tide and pressure gauge comparisons, respectively.

coastal regions resulting in the exclusion of some validation pairs, precluding the application of quality flags. Figure 2a shows a linear regression fitted to the paired gauge measurements with a slope of 0.99. An RMSE of 0.13 m quantifies the average measurement uncertainty, while the consistent STD of 0.13 m across all stations and low bias demonstrates reliable performance in one of Earth's most extreme tidal environments. Offshore, ADCP sensors recorded water level with a higher RMSE of 0.35 m (Figure 2d), attributable to floating mooring oscillations induced by local waves and currents. While 10-min averaging of high-frequency height data reduces surface wave variability, it introduces a temporal mismatch with SWOT overpasses since high-frequency fluctuations within that interval prevents reliable temporal interpolation. Overall, the analysis confirms SWOT's ability to capture the full spectrum of tidal variations with accuracy comparable to in situ measurements, maintaining a consistently small bias across tidal ranges (4–12 m). This performance is particularly notable given the complex interactions between tidal forces, wind-induced waves, and bathymetric features in the coastal environment.

3.2. Spatial Comparison Between LiDAR and SWOT

The spatial accuracy of SWOT WSE was evaluated using LiDAR measurements at both pixel and raster scales. Validation utilized 25,871 SWOT raster grids and 838,569 pixels, benchmarked against ~446 million LiDAR

points. Quality assessment revealed 74% of raster grids classified as nominal, 9% as suspect, and 17% as degraded. For PIXC data, ∼90% were nominal and ∼10% degraded. The high proportion of nominal data (74%–90%) suggests validation should yield reliable results if quality indicators accurately reflect actual data quality.

Sensitivity of the SWOT performance to variations in quality flag reveals minor RMSE fluctuations (Tables S2–S4 in Supporting Information S1), indicating negligible impact on validation in this study area, though effects may intensify in regions with more degraded data. Similarly, temporal offsets of ±10–60 s between SWOT and LiDAR acquisitions showed no statistically significant effect on performance (Figure 3e). Moreover, buffer radii ranging from 10 to 40 m centered on each pixel demonstrated minimal impact; while larger radii reduced LiDAR measurement variability (Figure S4 and Table S4 in Supporting Information S1), the RMSE remained stable, underscoring the robustness of spatial averaging. These findings confirm the site-specific reliability of SWOT data under tested conditions and self-reported quality flags while highlighting contextual dependencies for broader applications.

LiDAR-derived WSE were compared against SWOT Raster for each 100 m grid. Figure 3a employs LiDAR data with a ±60 s temporal offset relative to the SWOT overpass, while Figure 3c incorporates LiDAR data corrected via the NEMO-UK500 model. Linear regression reveals near-ideal proportionality between data sets, with slopes of 1.0 (uncorrected) and 1.01 (corrected) and a consistent intercept of −0.07 m. Statistical agreement is robust for both analyses, as evidenced by RMSE values of 0.16 m (uncorrected) and 0.17 m (corrected). The marginal histogram (top axis) further quantifies residuals (SWOT–LiDAR), showing ∼98% of errors within ±0.35 m. A left-skewed distribution underscores LiDAR's systematic tendency to report marginally higher WSE values, likely due to its superior spatial resolution (∼0.5 m) that captures fine-scale wave dynamics and surface heterogeneities. Additionally, the absence of some wave troughs in the LiDAR data may aggravate this discrepancy (Figure 1b).

Figure 3b (uncorrected, ±60 s offset) and Figure 3d (corrected) compare SWOT PIXC with LiDAR using a 10 m radius surrounding each SWOT pixel. The vertical distribution in these scatter plots indicates significant variability in PIXC WSE, with LiDAR variability smoothed through radius averaging and distribution narrowing as radius increases from 10 to 40 m (Figure S4 in Supporting Information S1). Despite a determination coefficient of 0.98, the analysis shows increased variability with RMSE values of 0.43/0.40 m and STD of 0.40/0.37 m. Scatter outliers exceeding 0.5 m contribute to a bias of −0.14 m (Figure 3d), improving to −0.08 m when considering the 82.6% of pixel pairs within ±0.5 m. This increased variability demonstrates the trade-off in SWOT's finer spatial resolution, where greater spatial detail comes at the cost of increased susceptibility to localized measurement uncertainties.

The cumulative distribution for the NEMO-UK500-corrected LiDAR data in Figures 3e and 3f reveal scale-dependent error patterns. Raster-scale differences exhibit a steeper gradient around the median compared to the more gradual slope at the pixel scale, resulting in superior performance metrics for Raster (RMSE: 0.16 m, Bias: −0.07 m) versus PIXC (RMSE: 0.40 m, Bias: −0.14 m). Further analysis within 1 km^2 areas shows that the STD between SWOT and LiDAR measurements remains within 0.09 m (Figure S3 in Supporting Information S1), confirming SWOT achieves its target accuracy specification, even in a challenging coastal environment.

3.3. Spatial Error Characteristics of SWOT WSE

Figure 4a shows a typical spatial error map (SWOT–LiDAR) with coherent ∼50 m banding and residuals up to ±2 m. This pattern arises because SWOT's interferometric sampling interval can intersect wave trains, alternately hitting crests and troughs; slight timing or geolocation offsets (e.g., 0.5 arcmin geoid offset issue in Version C) relative to LiDAR then yield successive over- and underestimates. Strong tidal currents and variable bathymetry further alter wave speeds and slopes along the channel, reinforcing these bands.

Variogram analysis of SWOT–LiDAR WSE residuals were performed by binning residual pairs into 20–200 m separation bins at 0.25 m intervals and computing semivariance as half the mean squared difference within each bin. The variogram analysis shows cross-estuary flights with semivariance rising from ∼20 to 50 m distance and stabilizing near ∼0.1 m^2 (Figure 4b), indicating small, quickly decorrelating errors, while along-estuary flights exhibit higher semivariance (∼0.2–0.4 m^2) with cyclical, non-stabilizing patterns (Figure 4c). This reflects Bristol Channel dynamics: cross-estuary tracks sample relatively uniform water levels transversely, yielding low, predictable semivariance, whereas along-estuary tracks encounter persistent tidal slopes, strong currents,

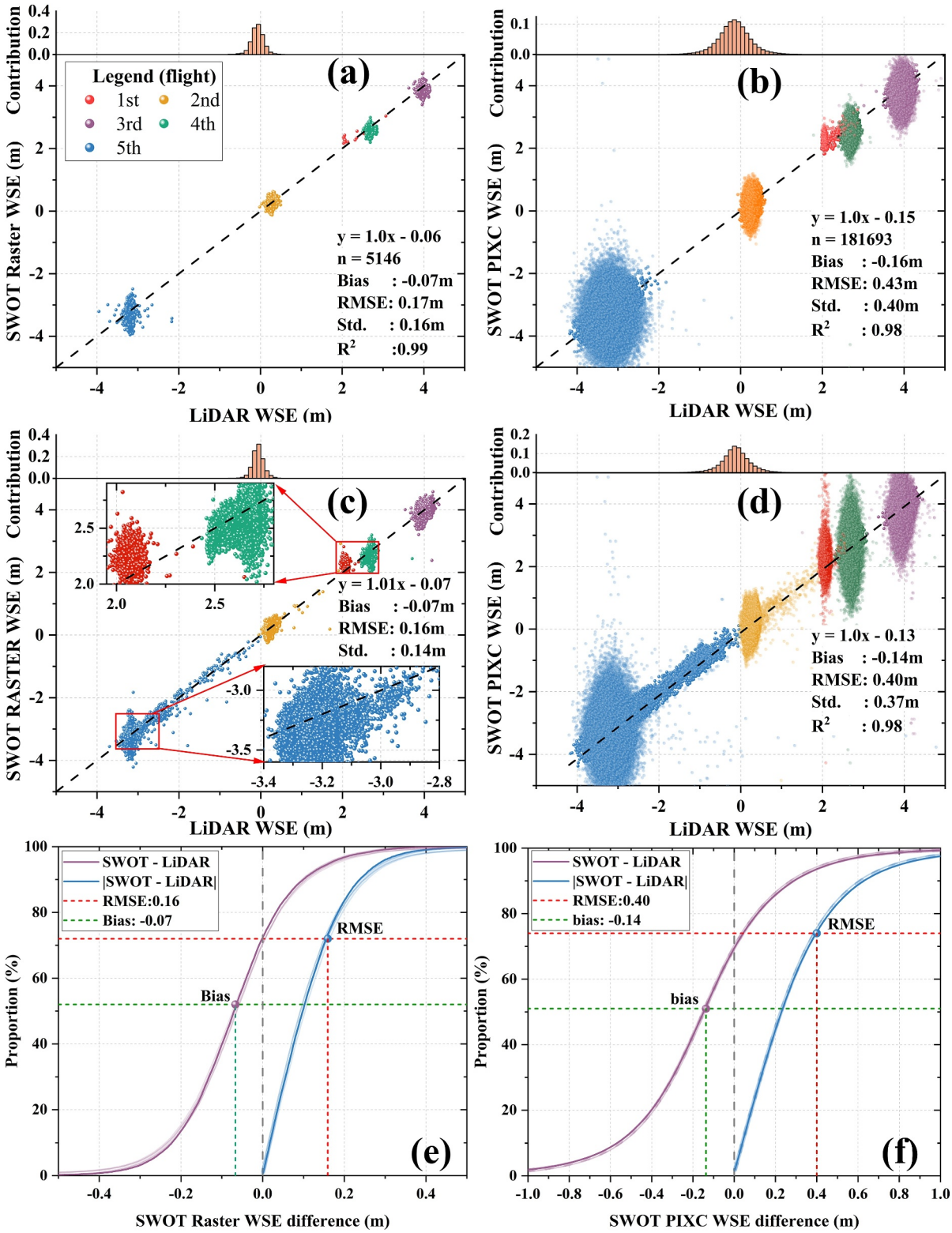

Figure 3. Validation of Surface Water and Ocean Topography water surface elevation (WSE) spatial accuracy using LiDAR data. (a) LiDAR versus Raster within ±60s of overpass. (b) LiDAR versus PIXC within 10 m radius and ±60 s of overpass. (c) NEMO-UK500 corrected LiDAR versus Raster (±60 s). (d) NEMO-UK500 corrected LiDAR versus PIXC (10 m radius, ±60 s). Panels (e, f) CDFs of SWOT–LiDAR WSE differences at raster and pixel scales; shadow in panel (e) shows time sensitivity while panel (f) shows radius sensitivity.

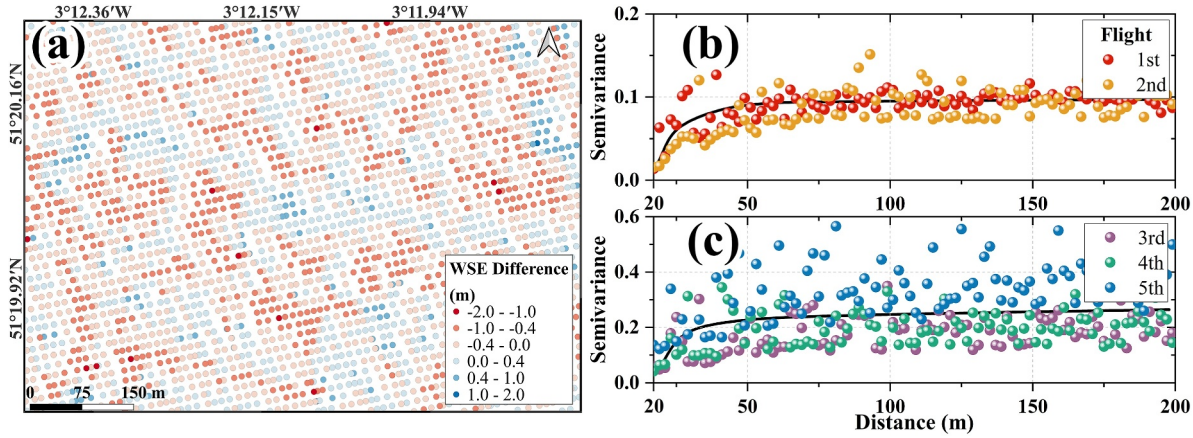

Figure 4. Spatial characteristics of water surface elevation differences (SWOT–LiDAR), with semivariance in (b) cross-estuary and (c) along-estuary directions.

bathymetry-driven gradients, and wave trains aligned with the sampling direction. These factors produce alternating over- and underestimates that reinforce coherent spatial structures and elevate semivariance.

Beyond this physical hydrodynamic effect, error patterns depend on SWOT swath orientation: cross-estuary (parallel to the SWOT swath) yields more stable, predictable errors, while along-estuary shows greater variability and complex correlations. This reflects SWOT's sensitivity to the geometry between its sampling direction and the waterbody orientation (Domeneghetti et al., 2018). Lower semivariance in the cross-estuary direction likely arises from better alignment with the swath, whereas higher variability along-estuary stems from across-track sampling challenges compounded by tidal currents and bathymetry-driven slopes.

4. Discussion and Conclusions

This study evaluates SWOT WSE measurements in a complex coastal setting using LiDAR, ADCP-mounted pressure sensors, and shore tide gauges. SWOT reliably tracks water level variations under 4–12 m tidal ranges with STD of 0.13 m for tide gauges and 0.09–0.14 m for spatially averaged LiDAR comparisons (Table S5 in Supporting Information S1). Critically, SWOT maintains sub-decimeter accuracy within 1–2 km of irregular coastlines in a challenging coastal environment, whereas traditional nadir altimetry experiences land contamination within 1–5 km of coastlines (Dinardo et al., 2018; Passaro et al., 2014; Peng et al., 2024) despite advanced SAR mode and retracking algorithms. Beyond improved coastal performance, SWOT's 2D swath coverage (~120 km width) resolves spatial WSE variability fundamentally inaccessible to along-track altimetry.

SWOT PIXC measurements show systematic spatial errors of ±2 m, with variogram analysis revealing clear anisotropy: cross-estuary errors decorrelate over shorter distances, while along-estuary errors exhibit larger magnitudes and cyclical, non-stabilizing patterns. These patterns arise because SWOT's oblique radar incidence interacts with tidal dynamics, bathymetry, shoreline morphology, and wave fields differently than near nadir-looking LiDAR. In the cross-estuary direction, shorter correlation lengths suggest lateral averaging can effectively reduce uncertainty; in the along-estuary direction, persistent correlations demand averaging approaches that account for longer-range error structure. Consequently, coastal SWOT processing should use anisotropic error models that consider: (a) the geometric alignment between SWOT's swath and channel orientation, (b) the influence of tidal and intertidal morphology on radar returns, and (c) the differing spatial scales of error correlation in cross-versus along-estuary directions.

SWOT products evolve through successive versions as processing algorithms and calibration parameters are refined. This study used Version C data from the Cal/Val phase, which should translate well to routine operations since the fast-sampling orbit altitude differs only marginally from the nominal science orbit (https://swot.jpl.nasa.gov/system/documents/files/2244_2244_D-75724_SWOT_Cal_Val_Plan_Initial_20180129u.pdf), although absolute error magnitudes will likely improve. However, Version C contains known issues including a 0.5 × 0.5 arcmin geoid interpolation offset that introduces spatial biases (typically <5 cm over our study area) and residual water-fraction/SSH fill-value artifacts that may contribute to larger errors observed in this analysis.

While Version D forward-processing products began in April 2025, with Cal/Val reprocessing expected by 2026, precise error reductions cannot yet be quantified. Nevertheless, our validation using nominal-quality data and excluding measurements within 50 m of the shore demonstrates that in complex estuarine environments SWOT meets its <0.1 m error requirement over 1 km^2 areas, providing a baseline for future studies to quantify processing improvements.

We conclude that SWOT demonstrates viable capabilities for coastal WSE monitoring, with accuracy suitable for many applications when appropriate filtering and processing strategies are applied. The combination of LiDAR, ADCP-mounted pressure sensor, and gauge measurements provides complementary validation approaches, offering unprecedented insights into both spatial and temporal error characteristics at both pixel and aggregated scales. This validation approach establishes a robust framework for future SWOT calibration efforts in coastal environments and suggests that integrated use of multiple reference data sets may be necessary for the comprehensive validation of satellite-based WSE measurements in complex coastal settings.

Conflict of Interest

The authors declare no conflicts of interest relevant to this study.

Data Availability Statement

Tide gauge data for Newport, Avonmouth Portbury, and Hinkley PointC are publicly available from the British Oceanographic Data Centre (BODC, https://www.bodc.ac.uk/data/hosted_data_systems/sea_level/uk_tide_gauge_network/). The Penarth pressure gauge data are open access through the Channel Coastal Observatory (https://coastalmonitoring.org) and Welsh Coastal Monitoring Centre (https://www.wcmc.wales). The GNSS-IR, ADCP, and LiDAR data used in this paper is available through the British Oceanographic Data Centre (Bates et al., 2026).

Acknowledgments
The SWOT-UK project was funded by NERC/UK Space Agency grants NE/V009168/1 (NOC), NE/V009125/1 (Bristol), and NE/V009109/1 (Bangor). The NEMO-UK500 model was developed by the CHAMFER project (NE/W004992/1). LiDAR overflights on 7 and 25 April 2023 were conducted by England's Environment Agency Geomatics Unit. We thank the National Coastwatch Institution for hosting GNSS-IR gauges, and the anonymous reviewers for their constructive feedback.

References

Alsdorf, D. E., Rodríguez, E., & Lettenmaier, D. P. (2007). Measuring surface water from space. *Reviews of Geophysics*, *45*(2). https://doi.org/10.1029/2006RG000197

Altenau, E. H., Pavelsky, T. M., Moller, D., Lion, C., Pitcher, L. H., Allen, G. H., et al. (2017). AirSWOT measurements of river water surface elevation and slope: Tanana River, AK. *Geophysical Research Letters*, *44*(1), 181–189. https://doi.org/10.1002/2016gl071577

AVISO/DUACS. (2025). SWOT Level-3 KaRIn low rate SSH unsmoothed (v2.0.1) [Dataset]. https://doi.org/10.24400/527896/A01-2024.003

Bates, P., Neal, J., & Rong, Y. (2026). High-resolution airborne light detection and ranging (LiDAR) scans of the Bristol Channel and Severn Estuary, UK (April - June 2023) [Dataset]. *NERC EDS British Oceanographic Data Centre NOC*. https://doi.org/10.5285/42c2a851-75df-8c8b-e063-7086abc078c3

Birol, F., Léger, F., Passaro, M., Cazenave, A., Niño, F., Calafat, F. M., et al. (2021). The X-TRACK/ALES multi-mission processing system: New advances in altimetry towards the coast. *Advances in Space Research*, *67*(8), 2398–2415. https://doi.org/10.1016/j.asr.2021.01.049

Calafat, F. M., Wahl, T., Tadesse, M. G., & Sparrow, S. N. (2022). Trends in Europe storm surge extremes match the rate of sea-level rise. *Nature*, *603*(7903), 841–845. https://doi.org/10.1038/s41586-022-04426-5

Cipollini, P., Calafat, F. M., Jevrejeva, S., Melet, A., & Prandi, P. (2017). Monitoring Sea level in the coastal zone with satellite altimetry and tide gauges. *Surveys in Geophysics*, *38*(1), 33–57. https://doi.org/10.1007/s10712-016-9392-0

Dibarboure, G., Anadon, C., Briol, F., Cadier, E., Chevrier, R., Delepoulle, A., et al. (2024). Blending 2D topography images from SWOT into the altimeter constellation with the Level-3 multi-mission DUACS system. *EGUsphere*, *2024*, 1–64. https://doi.org/10.5194/egusphere-2024-1501

Dinardo, S., Fenoglio-Marc, L., Becker, M., Scharroo, R., Fernandes, M. J., Staneva, J., et al. (2021). A RIP-based SAR retracker and its application in North East Atlantic with Sentinel-3. *Advances in Space Research*, *68*(2), 892–929. https://doi.org/10.1016/j.asr.2020.06.004

Dinardo, S., Fenoglio-Marc, L., Buchhaupt, C., Becker, M., Scharroo, R., Joana Fernandes, M., & Benveniste, J. (2018). Coastal SAR and PLRM altimetry in German Bight and West Baltic Sea. *Advances in Space Research*, *62*(6), 1371–1404. https://doi.org/10.1016/j.asr.2017.12.018

Domeneghetti, A., Schumann, G. J. P., Frasson, R. P. M., Wei, R., Pavelsky, T. M., Castellarin, A., et al. (2018). Characterizing water surface elevation under different flow conditions for the upcoming SWOT mission. *Journal of Hydrology*, *561*, 848–861. https://doi.org/10.1016/j.jhydrol.2018.04.046

Environment Agency. (2024). Environment agency real time flood-monitoring API. Retrieved from https://environment.data.gov.uk/flood-monitoring/doc/reference

Fenoglio, L., Dinardo, S., Uebbing, B., Buchhaupt, C., Gärtner, M., Staneva, J., et al. (2021). Advances in NE-Atlantic coastal sea level change monitoring by delay Doppler altimetry. *Advances in Space Research*, *68*(2), 571–592. https://doi.org/10.1016/j.asr.2020.10.041

Fu, L.-L., & Cazenave, A. (2000). *Satellite altimetry and Earth sciences: A handbook of techniques and applications*. Elsevier.

Fu, L. L., Pavelsky, T., Cretaux, J. F., Morrow, R., Farrar, J. T., Vaze, P., et al. (2024). The surface water and ocean topography mission: A breakthrough in radar remote sensing of the ocean and land surface water. *Geophysical Research Letters*, *51*(4), e2023GL107652. https://doi.org/10.1029/2023gl107652

Greaves, M. (2016). OSGM15 and OSTN15. *Geomatics World*, *32*(33), 1–5.

Hart-Davis, M. G., Andersen, O. B., Ray, R. D., Zaron, E. D., Schwatke, C., Arildsen, R. L., et al. (2024). Tides in complex coastal regions: Early case studies from wide-swath SWOT measurements. *Geophysical Research Letters*, *51*(20), e2024GL109983. https://doi.org/10.1029/2024gl109983

Hauer, M. E., Hardy, D., Kulp, S. A., Mueller, V., Wrathall, D. J., & Clark, P. U. (2021). Assessing population exposure to coastal flooding due to sea level rise. *Nature Communications*, *12*(1), 6900. https://doi.org/10.1038/s41467-021-27260-1

Jafarzadegan, K., Moradkhani, H., Pappenberger, F., Moftakhari, H., Bates, P., Abbaszadeh, P., et al. (2023). Recent advances and new frontiers in riverine and coastal flood modeling. *Reviews of Geophysics*, *61*(2), e2022RG000788. https://doi.org/10.1029/2022rg000788

Kleinherenbrink, M., Naeije, M., Slobbe, C., Egido, A., & Smith, W. (2020). The performance of CryoSat-2 fully-focussed SAR for inland water-level estimation. *Remote Sensing of Environment*, *237*, 111589. https://doi.org/10.1016/j.rse.2019.111589

Laignel, B., Ayoub, N., Birol, F., Brown, S., Chao, Y., Cornuelle, B., et al. (2015). Issues and SWOT contribution in the coastal zones and estuaries White Paper. *SWOT White Papers*.

Lichtman, I. D., Bell, P., Williams, S., Gommenginger, C., Banks, C., Calafat, F., & Brown, J. (2024). Water level data from the Bristol Channel and Severn Estuary and river region for validation of satellite altimeters, 2012-2023 (SWOT-UK project) [Dataset]. *NERC EDS British Oceanographic Data Centre NOC*. https://www.bodc.ac.uk/data/published_data_library/catalogue/10.5285/25129f9a-7369-9ab2-e063-7086abc05905

Lichtman, I. D., Bell, P. S., Gommenginger, C., Banks, C., Calafat, F. M., Brown, J., & Williams, S. D. P. (2025). Evaluating water levels from the surface water and ocean topography (SWOT) mission in a hyper-tidal coastal and estuarine environment. *Earth and Space Science*, *12*(7), e2024EA004104. https://doi.org/10.1029/2024ea004104

Lyddon, C., Brown, J. M., Leonardi, N., & Plater, A. J. (2018). Flood hazard assessment for a hyper-tidal Estuary as a function of tide-surge-morphology interaction. *Estuaries and Coasts*, *41*(6), 1565–1586. https://doi.org/10.1007/s12237-018-0384-9

O'Loughlin, F. E., Neal, J., Yamazaki, D., & Bates, P. D. (2016). ICESat-derived inland water surface spot heights. *Water Resources Research*, *52*(4), 3276–3284. https://doi.org/10.1002/2015wr018237

Passaro, M., Cipollini, P., Vignudelli, S., Quartly, G. D., & Snaith, H. M. (2014). ALES: A multi-mission adaptive subwaveform retracker for coastal and open ocean altimetry. *Remote Sensing of Environment*, *145*, 173–189. https://doi.org/10.1016/j.rse.2014.02.008

Peng, F., Deng, X., & Shen, Y. (2024). Assessment of Sentinel-6 SAR mode and reprocessed Jason-3 sea level measurements over global coastal oceans. *Remote Sensing of Environment*, *311*, 114287. https://doi.org/10.1016/j.rse.2024.114287

Salameh, E., Desroches, D., Deloffre, J., Fjørtoft, R., Mendoza, E. T., Turki, I., et al. (2024). Evaluating SWOT's interferometric capabilities for mapping intertidal topography. *Remote Sensing of Environment*, *314*, 114401. https://doi.org/10.1016/j.rse.2024.114401

Schlembach, F., Passaro, M., Dettmering, D., Bidlot, J., & Seitz, F. (2022). Interference-sensitive coastal SAR altimetry retracking strategy for measuring significant wave height. *Remote Sensing of Environment*, *274*, 112968. https://doi.org/10.1016/j.rse.2022.112968

Schuerch, M., Spencer, T., Temmerman, S., Kirwan, M. L., Wolff, C., Lincke, D., et al. (2018). Future response of global coastal wetlands to sea-level rise. *Nature*, *561*(7722), 231–234. https://doi.org/10.1038/s41586-018-0476-5

SWOT. (2024a). SWOT level 2 water mask pixel cloud data product [Dataset]. Retrieved from https://podaac.jpl.nasa.gov/dataset/SWOT_L2_HR_PIXC_2.0

SWOT. (2024b). SWOT level 2 water mask raster image data product [Dataset]. Retrieved from https://podaac.jpl.nasa.gov/dataset/SWOT_L2_HR_Raster_2.0

Toimil, A., Losada, I. J., Álvarez-Cuesta, M., & Le Cozannet, G. (2023). Demonstrating the value of beaches for adaptation to future coastal flood risk. *Nature Communications*, *14*(1), 3474. https://doi.org/10.1038/s41467-023-39168-z

Turki, I., Laignel, B., Chevalier, L., Costa, S., & Massei, N. (2015). On the investigation of the sea-level variability in coastal zones using SWOT satellite mission: Example of the eastern English Channel (western France). *IEEE Journal of Selected Topics in Applied Earth Observations and Remote Sensing*, *8*(4), 1564–1569. https://doi.org/10.1109/JSTARS.2015.2419693

Uncles, R. J. (2010). Physical properties and processes in the Bristol Channel and Severn Estuary. *Marine Pollution Bulletin*, *61*(1–3), 5–20. https://doi.org/10.1016/j.marpolbul.2009.12.010

Vignudelli, S., Scozzari, A., Abileah, R., Gómez-Enri, J., Benveniste, J., & Cipollini, P. (2019). Water surface elevation in coastal and inland waters using satellite radar altimetry. In *Extreme hydroclimatic events and multivariate hazards in a changing environment* (pp. 87–127).

Williams, S. D. P., Bell, P. S., McCann, D. L., Cooke, R., & Sams, C. (2020). Demonstrating the potential of low-cost GPS units for the remote measurement of tides and water levels using interferometric reflectometry. *Journal of Atmospheric and Oceanic Technology*, *37*(10), 1925–1935. https://doi.org/10.1175/JTECH-D-20-0063.1

Zlinszky, A., Boergens, E., Glira, P., & Pfeifer, N. (2017). Airborne laser scanning for calibration and validation of inshore satellite altimetry: A proof of concept. *Remote Sensing of Environment*, *197*, 35–42. https://doi.org/10.1016/j.rse.2017.04.027

References From the Supporting Information

Desai, S. (2018). *Surface water and ocean topography mission project-science requirements document*. JPL document D-61923. Jet Propulsion Laboratory. Retrieved from https://swot.jpl.nasa.gov/system/documents/files/2176_2176_D-61923_SRD_Rev_B_20181113.pdf

Jevrejeva, S., Calafat, F. M., De Dominicis, M., Hirschi, J. J. M., Mecking, J. V., Polton, J. A., et al. (2024). Challenges, advances and opportunities in regional sea level projections: The role of ocean-shelf dynamics. *Earth's Future*, *12*(8), e2024EF004886. https://doi.org/10.1029/2024ef004886

Lyard, F. H., Allain, D. J., Cancet, M., Carrère, L., & Picot, N. (2021). FES2014 global ocean tide atlas: Design and performance. *Ocean Science*, *17*(3), 615–649. https://doi.org/10.5194/os-17-615-2021

Madec, G., & the NEMO System Team. (2024). NEMO ocean engine reference manual. *Zenodo*.

O'Dea, E., Bell, M. J., Coward, A., & Holt, J. (2020). Implementation and assessment of a flux limiter based wetting and drying scheme in NEMO. *Ocean Modelling*, *155*, 101708. https://doi.org/10.1016/j.ocemod.2020.101708

Warner, J. C., Defne, Z., Haas, K., & Arango, H. G. (2013). A wetting and drying scheme for ROMS. *Computers & Geosciences*, *58*, 54–61. https://doi.org/10.1016/j.cageo.2013.05.004